Journal of Computational Physics 305 (2016) 575–588

Contents lists available at ScienceDirect

Journal of Computational Physics

www.elsevier.com/locate/jcp

An asymptotic preserving Monte Carlo method for the multispecies Boltzmann equation

Bin Zhang [a,b], Hong Liu [a,*], Shi Jin [b,c]

[a] J.C. Wu Center for Aerodynamics, School of Aeronautics and Astronautics, Shanghai Jiao Tong University, 800 Dong Chuan Road, Shanghai, 200240, China
[b] Department of Mathematics, Institute of Natural Science, MOE-LSEC and SHL-MAC, Shanghai Jiao Tong University, 800 Dong Chuan Road, Shanghai 200240, China
[c] Department of Mathematics, University of Wisconsin-Madison, 480 Lincoln Drive, Madison, WI 53706, USA

ARTICLE INFO

Article history:
Received 16 June 2015
Received in revised form 2 November 2015
Accepted 3 November 2015
Available online 11 November 2015

Keywords:
Multispecies Boltzmann equation
Asymptotic preserving scheme
DSMC
Multiscale flow

ABSTRACT

An asymptotic preserving (AP) scheme is efficient in solving multiscale kinetic equations with a wide range of the Knudsen number. In this paper, we generalize the asymptotic preserving Monte Carlo method (AP-DSMC) developed in [25] to the multispecies Boltzmann equation. This method is based on the successive penalty method [26] originated from the BGK-penalization-based AP scheme developed in [7]. For the multispecies Boltzmann equation, the penalizing Maxwellian should use the unified Maxwellian as suggested in [12]. We give the details of AP-DSMC for multispecies Boltzmann equation, show its AP property, and verify through several numerical examples that the scheme can allow time step much larger than the mean free time, thus making it much more efficient for flows with possibly small Knudsen numbers than the classical DSMC.

1. Introduction

Boltzmann type kinetic equations with a wide range of spatial and temporal scales arise in many important applications from astronautics, nuclear engineering, semiconductor device modeling to plasma physics. Take the space shuttle reentry problem for example, the vehicle will pass from free streaming, rarefied gas, transition to continuum regimes, during which the particle mean free path varies from $O(1)$ to about 10^{-8} meters. Numerical simulation of such multiscale problems is daunting. Another challenge comes from the high dimensionality of such phase space models which are six dimensional equations plus time. Direct Simulation Monte-Carlo (DSMC) is the most popular choice [1], yet it suffers from huge computational expenses since one needs to resolve the small mean free time (or Knudsen number) temporally when the vehicles are near the earth, in the so-called fluid dynamic regime. Although in this regime one could use the macroscopic models such as the compressible Euler or Navier–Stokes equations, these equations are invalid in the rarified regime at which the Knudsen number is large.

In recent years, the development of asymptotic-preserving schemes [10], for multiscale kinetic and transport equations, has seen a rapid growth [11,6]. The idea of AP schemes is to develop the schemes that preserve the asymptotic transition from the kinetic models to the macroscopic fluid or diffusion models, which also need to be efficient for time discretization.

* Corresponding author.
E-mail address: Hongliu@sjtu.edu.cn (H. Liu).

http://dx.doi.org/10.1016/j.jcp.2015.11.006
0021-9991/

Table 1
Dimensionless variables and the corresponding reference values.

Name	Physical variable	Dimensionless variable	Reference value
Position	$\tilde{x}$	x	L
Velocity	$\tilde{v}$	v	$\bar{c}=\sqrt{\frac{8kT}{\pi m}}$
Time	$\tilde{t}$	t	$\tau=L/\bar{c}$
Relative velocity	$\tilde{g}$	g	$\bar{g}=\sqrt{2}\bar{c}$
Collision cross-section	$\tilde{\sigma}$	σ	πd^2
Distribution function	$\tilde{f}$	f	$f_c=n/C^3$

In particular one favors a scheme in which the time step is independent of the mean free time (or Knudesn number) [10]. These AP schemes are attractive since they do not need the coupling of kinetic and fluid models in the domain-decomposition setting [3,4,9,13,2,15].

For the multiscale Boltzmann equation, a time efficient AP scheme was proposed by Filbet–Jin [7], with the idea of penalizing the nonlinear, nonlocal Boltzmann collision operator by the BGK relaxation operator whose implicit discretization can be implemented *explicitly*. The AP property and positivity can be strengthened by a successive penalization as proposed by Yan and Jin [26]. Such idea can be used for multiscale Boltzmann equation as was done by Jin and Li [12]. Another approach is based on exponential Runge–Kutta approach, see [16,8]. See also [17]. Attempts to develop AP Monte Carlo methods can also be found in [22,23,21].

In this article, we extend the AP-DSMC developed in [25] for single species Boltzmann equation to the multispecies Boltzmann equation. This work is mainly motivated by developing highly efficient Monte carlo scheme for multiscale flow fields related to reentry problems or hypersonic vehicles [18,14] where the gas is usually considered as a binary mixture of Oxygen and Nitrogen. For the multispecies system, the conservation laws break down for each single species. When using the BGK penalization approach, the *unified* Maxwellian which depends on the mean velocity and mean temperature is found to be suitable in the penalization [12]. We illustrate the AP property of our scheme, and in addition, several multispecies examples are used to test our proposed method which will be compared with the conventional DSMC. The numerical results show that the proposed method not only has the ability of capturing the macroscopic behavior in flow dynamic regimes, as well as the rarified regime, more importantly, it is much more efficient than DSMC in the cases of stiff collision process since the AP-DSMC does not need to resolve the small Knudsen number numerically. The numerical results demonstrate that the proposed method is very promising in engineering applications.

The rest of the paper is organized as follows. In Section 2, we briefly describe the Boltzmman equation for the multispecies system and its basic properties. Next, we give details of the AP-DSMC scheme for the multispecies Boltzmman equation in Section 3 and discuss its asymptotic behavior in the fluid dynamic regime. We present several examples to show the performance of the proposed method in Section 4 and make conclusive remarks in Section 5.

2. The multispecies models

2.1. The multispecies Boltzmann equation

The multispecies Boltzmann equation describes the time evolution of the density distribution of a dilute gas that has more than two components whose particles usually have different masses. In this paper, we are interested in developing efficient numerical scheme for the nonlinear N-species Boltzmann equation which is given by

$$\frac{\partial \tilde{f}_i}{\partial \tilde{t}}+\tilde{v}\cdot\nabla_{\tilde{x}}\tilde{f}_i=\tilde{Q}_i\left(\tilde{f},\tilde{f}\right),\ t\geq 0,\ \left(\tilde{x},\tilde{v}\right)\in R^d\times R^d,\ 1\leq i\leq N, \tag{1}$$

where $\tilde{f}_i=\tilde{f}\left(\tilde{x},\tilde{v},\tilde{t}\right)$ is a nonnegative distribution function of the i-th species which move at time $\tilde{t}$, position $\tilde{x}$ with velocity $\tilde{v}$. $\tilde{Q}_i$ is the collision operator to be defined later. Some useful dimensionless variables and the corresponding reference values are listed in Table 1, where d and n denote the molecular diameter and the number density respectively. $k=1.380622\times 10^{23}$ is Boltzmann constant. By introducing dimensionless quantities (see Table 1), Eq. (1) can be rewritten in a dimensionless form,

$$\frac{L}{\tau\bar{c}}\frac{\partial f_i}{\partial t}+v\cdot\nabla_x f_i=\frac{\tilde{\sigma}ngL}{\bar{c}}Q_i\left(f,f\right),\ t\geq 0,\ x\in R^{d_x},\ v\in R^{d_v},\ 1\leq i\leq N, \tag{2}$$

where $St=L\,/\,(\tau\bar{c})$ is Strouhal number which is usually set to unity. Given the relation of $\frac{\bar{c}}{\tilde{\sigma}ng}=\frac{\bar{c}}{\nu}=\lambda$, the Knudsen number $\varepsilon=\lambda\,/\,L$ defined as the ratio of the mean free path λ over a typical length scale L can be obtained to measure the rarefiedness of the gas. Therefore, a dimensionless form of the equation is given as follows

$$\frac{\partial f_i}{\partial t}+v\cdot\nabla_x f_i=\frac{1}{\varepsilon}Q_i\left(f,f\right),\ t\geq 0,\ x\in R^{d_x},\ v\in R^{d_v},\ 1\leq i\leq N. \tag{3}$$

In Eq. (3), the bilinear collision term is given by

$$\begin{cases} Q_i(f,f) = \sum_{k=1}^{N} Q_{ik}(f,f), \\ Q_{ik}(f,f)(v) = \int_{S^{d_v-1}} \int_{R^{d_v}} \left(f_i(v') f_k(v'_*) - f_i(v) f_k(v_*) \right) \sigma_{ik}(|v-v_*|,\omega)\, dv_* d\omega, \end{cases} \tag{4}$$

where $f = (f_1, f_2, \ldots, f_N)^T$, ω is a unit vector, and S^{d_v-1} is the unit sphere defined in R^{d_v} space. σ_{ik} denotes the symmetric collision kernel ($\sigma_{ik} = \sigma_{ki}$) which depends on the model of forces between particles. v, v_* are pre-collisional velocities, v', v'_* are post-collisional velocities. Define the relative velocity $g = v - v_*$, the post-collisional velocities satisfy:

$$\begin{cases} v' = v - \frac{\mu_{ik}}{m_i}(g - |g|\omega) \\ v'_* = v_* + \frac{\mu_{ik}}{m_k}(g - |g|\omega) \end{cases}; \quad \mu_{ik} = \frac{m_i m_k}{m_i + m_k}, \tag{5}$$

where μ_{ik} is the reduced mass, and m_i, m_k are the mass for species i and k respectively. These equations are based on momentum and energy conservations

$$\begin{cases} m_i v + m_k v_* = m_i v' + m_k v'_*, \\ m_i v v + m_k v_* v_* = m_i v' v' + m_k v'_* v'_*. \end{cases} \tag{6}$$

The collision operator $Q_{ik}(f,f)$ can also be split into two parts

$$\begin{cases} Q_{ik}(f,f)(v) = Q_{ik}^{+}(f,f) - f_i Q_{ik}^{-}(f), \\ Q_{ik}^{+}(f,f) = \int_{S_+^{d-1}} \int_d \sigma_{ik}(|v-v_*|,\omega)\, f_i(v') f_k(v'_*)\, dv_* d\omega, \\ Q_{ik}^{-}(f,f) = \int_{S_+^{d-1}} \int_d \sigma_{ik}(|v-v_*|,\omega)\, f_k(v'_*)\, dv_* d\omega, \end{cases} \tag{7}$$

where Q_{ik}^{+} and Q_{ik}^{-} denote gain term and loss term respectively.

2.2. Properties of the multispecies Boltzmann equation

In d-dimensional space, the macroscopic quantities for species i, such as number density n_i, density ρ_i, average velocity u_i, temperature T_i, specific internal energy e_i, total energy E_i and heat flux q_i can be obtained by taking the moments:

$$\begin{cases} n_i = \int f_i dv; \ \rho_i = m_i n_i; \\ u_i = \frac{1}{n_i} \int v f_i dv; \ T_i = \frac{m_i}{n_i d} \int f_i |v-u_i|^2 dv; \\ e_i = \frac{d}{2} T_i = \frac{m_i}{2n_i} \int |v-u_i|^2 f_i dv; \\ E_i = \frac{1}{2}\rho_i u_i^2 + n_i e_i = \frac{m_i}{2} \int |v|^2 f_i; \\ q_i = \frac{1}{2} m_i \int (v-u_i)|v-u_i|^2 f_i dv. \end{cases} \tag{8}$$

Based on these quantities, the global quantities for the mixture: the number density n, the total mass density ρ, the mean velocity $\bar{u}$, the mean temperature $\bar{T}$, the internal energy $n\bar{e}$ and the total energy E can be obtained as

$$n = \sum_{i=1}^{N} n_i; \ \rho = \sum_{i=1}^{N} \rho_i; \ \bar{u} = \sum_{i=1}^{N} \frac{\rho_i u_i}{\rho}; \ E = n\bar{e} + \frac{1}{2}\rho|\bar{u}|^2 = \sum_{i=1}^{N} E_i; \ \bar{T} = \frac{2\bar{e}}{d}. \tag{9}$$

In the gas mixture system, for each species, only mass is conserved, while the momentum and energy are not. However, the total mass, momentum and energy are conserved:

$$\int m_i Q_i dv = 0; \ \sum_{i=1}^{N} \int m_i v_i Q_i dv = 0; \ \sum_{i=1}^{N} \int \frac{1}{2} m_i v_i^2 Q_i dv = 0. \tag{10}$$

When $\varepsilon = O(1)$, Eq. (3) is in kinetic regime. For $\varepsilon \ll 1$, the gas is near fluid dynamic regime. In particular, when $\varepsilon \to 0$, $Q_i(f) \to 0$, which implies

$$f_i = M_i = n_i \left(\frac{m_i}{2\pi \bar{T}} \right)^{\frac{d}{2}} \exp\left(-\frac{m_i |v-\bar{u}|^2}{2\bar{T}} \right). \tag{11}$$

The macroscopic quantities defined in Eq. (8) and Eq. (9) satisfy the compressible Euler equations.

$$\begin{cases} \partial_t \rho_i + \nabla_x \cdot (\rho_i \bar{u}) = 0, \\ \partial_t (\rho \bar{u}) + \nabla_x \cdot \left(\rho \bar{u} \otimes \bar{u} + n\bar{T} I\right) = 0, \\ \partial_t E + \nabla_x \cdot \left[\left(E + n\bar{T}\right) \bar{u}\right] = 0, \end{cases} \tag{12}$$

where I is the identity matrix. This is easy to verify formally since the local Maxwellian M_i satisfies $\int m_i M_i dv = \sum_{i=1}^{N} \int m_i v_i M_i dv = \sum_{i=1}^{N} \int \frac{1}{2} m_i v_i^2 M_i dv = 0$.

3. AP-DSMC scheme for the multispecies Boltzmann equation

In this section, the AP-DSMC scheme proposed in [25] is extended to solve the multispecies Boltzmann equation. The details of the numerical procedures of AP-DSMC are given as follows.

3.1. Time splitting of the multispecies Boltzmann equation

The multispecies Boltzmann equation is solved by a simple time splitting scheme:

$$\begin{cases} \frac{\partial f_i}{\partial t} + v \cdot \nabla_x f_i = 0, \\ \frac{\partial f_i}{\partial t} = \frac{1}{\varepsilon} Q_i (f, f). \end{cases} \tag{13}$$

The algorithm consists of two parts for each time step. In the first step (convection step), with a given original distribution function f^n, particles are convected by the first equation in (13) to give the distribution function f^*, which is taken as the initial data for the next collision step. Considering most numerical difficulties are coming from the second step (collision step given by the second equation of (13)), more description will be given below for this step.

3.2. The BGK-penalization in the space homogeneous equation

In order to handle the equation for all range of ε, one needs to handle the collision term efficiently when $\varepsilon \ll 1$ since the collision term becomes numerically stiff. The DSMC will need to take $\Delta t \ll O(\varepsilon)$. In order to overcome this difficulty, a BGK-penalization method with penalty term $P_i(f) = \beta (M_i - f_i)$ was introduced by Filbet and Jin [7]. The idea is to use $P_i(f)$ to penalize Q_i, and only treat $P_i(f)$ term implicitly *which can be solved explicitly*. The positive constant β is an upper bound of the coefficient of the loss term Q_i^-. For multispecies system, one has to choose a suitable Maxwellian for the BGK penalty function. As discussed in [12], one has to use Maxwellian (11) instead of the species Maxwellian which is (11) with $\bar{u}$ and $\bar{T}$ replaced by u_i and T_i, since the latter does not involve interactions between different species. Therefore, the collision equation can be written with the BGK-penalization term:

$$\frac{\partial f_i}{\partial t} = \underbrace{\frac{1}{\varepsilon} (Q_i (f, f) - P_i (f))}_{\text{less stiff}} + \underbrace{\frac{1}{\varepsilon} P_i (f)}_{\text{stiff}}. \tag{14}$$

On the right hand side, the first term is less stiff comparing with the second term. The time splitting scheme is applied to this equation again.

$$\begin{cases} \frac{\partial f_i}{\partial t} = \frac{1}{\varepsilon} (Q_i (f, f) - P_i (f)), \\ \frac{\partial f_i}{\partial t} = \frac{1}{\varepsilon} P_i (f). \end{cases} \tag{15}$$

The first equation is solved explicitly since it is less stiff:

$$\frac{f_i^{**} - f_i^*}{\Delta t} = \frac{1}{\varepsilon} \left(Q_i \left(f^*, f^*\right) - P_i \left(f^*\right)\right). \tag{16}$$

Time step for the second equation is divided into L subintervals and the same treatment as [26] is used for the equation with more stiff term:

$$\begin{cases} \frac{f_i^{n+1,1} - f_i^{**}}{\Delta t / L} = \frac{1}{\varepsilon} P_i^{n+1,1}, \\ \frac{f_i^{n+1,2} - f_i^{n+1,1}}{\Delta t / L} = \frac{1}{\varepsilon} P_i^{n+1,2}, \\ \qquad \cdots, \\ \frac{f_i^{n+1} - f_i^{n+1,L-1}}{\Delta t / L} = \frac{1}{\varepsilon} P_i^{n+1}, \end{cases} \tag{17}$$

where $P_i^{n+1,k} = \beta\left(M_i^{n+1,k} - f_i^{n+1,k}\right)$, $k = 1, \ldots, L$. Since $\overline{\rho}$, $\overline{u}$ and $\overline{T}$ are conserved for space homogeneous problem, one has $M_i^{n+1,1} = \ldots = M_i^{n+1} = M_i^{**}$, then the above equations can be rewritten as

$$\begin{cases} f_i^{n+1,1} = c f_i^{**} + (1-c) M_i^{**} \\ f_i^{n+1,2} = c f_i^{n+1,1} + (1-c) M_i^{**} \\ \ldots \\ f_i^{n+1} = c f_i^{n+1,L} + (1-c) M_i^{**} \end{cases} ; \quad c = \left(1 + \frac{\beta \Delta t}{\varepsilon L}\right)^{-1}. \tag{18}$$

A general formula for any L can be obtained as

$$f_i^{n+1} = c^L f_i^{**} + \left(1 - c^L\right) M_i^{**}. \tag{19}$$

Since $M_i^{**} = M_i^*$ and $\hat{Q}_i(f, f) = Q_i(f, f) + \beta f_i$, by combining Eq. (16) and Eq. (19) a much more clear form can be obtained as follows

$$\begin{aligned} f_i^{n+1} &= c^L \left[f_i^* + \frac{\Delta t}{\varepsilon}\left(Q_i\left(f^*, f^*\right) - P_i\left(f^*\right)\right)\right] + \left(1 - c^L\right) M_i^* \\ &= c^L f_i^* + c^L \frac{\Delta t}{\varepsilon} Q_i\left(f^*, f^*\right) - c^L \frac{\Delta t}{\varepsilon} \beta\left(M_i^* - f_i^*\right) + \left(1 - c^L\right) M_i^* \\ &= c^L f_i^* + c^L \frac{\Delta t \beta}{\varepsilon} \frac{\hat{Q}_i\left(f^*, f^*\right)}{\beta} + \left(1 - c^L - c^L \frac{\Delta t \beta}{\varepsilon}\right) M_i^* \\ &= b_0 f_i^* + b_1 \frac{\hat{Q}_i\left(f^*, f^*\right)}{\beta} + b_2 M_i^*. \end{aligned} \tag{20}$$

The weights in Eq. (20) are defined as

$$\begin{cases} b_0 = c_1 \\ b_1 = c_1 c_2 \\ b_2 = 1 - c_1 - c_1 c_2 \end{cases} ; \quad \begin{cases} c_1 = c^L = \left(1 + \frac{\mu}{L}\right)^{-L} \\ c_2 = \mu = \frac{\Delta t \beta}{\varepsilon} \end{cases}. \tag{21}$$

Note that the term $\hat{Q}_i\left(f^*, f^*\right) \Big/ \beta$ can be taken as a distribution function. It can be see that the scheme defined in Eq. (21) is positivity preserving since the weights b_i are nonnegative ($0 < c_1 < 1$ and $0 < c_2 < 1$) and satisfy $\sum_{i=0}^{2} b_i = 1$.

3.3. Asymptotic preserving property of the proposed scheme

As summarized by Jin [10], a scheme which has the following features can be considered as an AP scheme: First, it preserves the discrete analogy of the Chapman–Enskog expansion; second, implicit collision terms can be implemented efficiently. Therefore, the scheme defined in Eq. (20) has the asymptotic preserving property only if the nonnegative weights b_i satisfy the following condition.

$$\lim_{\mu \to \infty} b_0 = 0, \quad \lim_{\mu \to \infty} b_1 = 0, \quad \lim_{\mu \to \infty} b_2 = 1. \tag{22}$$

It can be deduced easily that the scheme cannot be considered as a strongly-AP scheme if $L = 1$ because it leads to $\lim_{\mu \to \infty} b_1 = 1$. (In [7] such a scheme is called a relaxed-AP scheme.) For any $L > 1$, the weights satisfy this condition and consequently $f_i^{n+1} \to M_i^*$ which leads to the correct Euler limit. Meanwhile, the scheme has the AP property in the sense that

$$f^n - M^n = \mathrm{O}(\varepsilon), \text{ for any } n \geq 1 \text{ and any initial data.} \tag{23}$$

In this paper, we choose $L = 2$ as in [25] because it can be considered as an optimal one in the view of computational efficiency. Fig. 1 shows the variations of weights b_i with different μ. It is obvious that b_2 tends to 1 while both b_0 and b_1 go to 0 if μ is large enough. As a matter of fact, the proposed scheme will become the exponential Runge–Kutta method (ExpRK) [5] which is also an AP scheme if $L \to \infty$. For the hydrodynamic limit, both the AP-DSMC and ExpRK reduce to a Euler solver ($b_0 = b_1 = 0$) and the computational costs are almost the same. However, for near-continuum regime it is evident that AP-DSMC is about 20% faster than ExpRK. The main reason is that b_2 of ExpRK is larger than that of AP-DSMC in the same typical simulations and the relaxation part (controlled by b_2) is usually more time-consuming comparing with the collision part. More detailed quantitative demonstration can be found in [25].

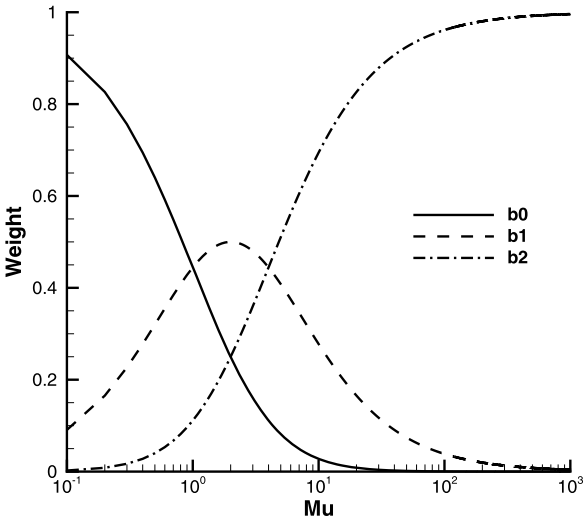

Fig. 1. Weights b_i of AP-DSMC with varying μ.

For cases with large μ, the conventional DSMC has to use $\Delta t \ll \varepsilon$, thus it spends most of computing time at solving collision process. Specifically, the computational cost of the collision treatments in DSMC is proportional to the number of dummy collision pairs N_c.

$$N_c = \frac{1}{2} N \rho \sigma_{\max} \Delta t \Big/ \varepsilon, \tag{24}$$

where N is the particle numbers in one cell. As for AP-DSMC, the computational cost is proportional to $(0.5b_1 + b_2)N$. It implies that the stiff collision process (corresponding to large μ) can be solved much more efficiently by AP-DSMC. In the next section, performance of AP-DSMC and DSMC will be compared in detail with different computational conditions.

3.4. The computational procedure

The computational procedure of the multispecies AP-DSMC during one time step can be summarized as:

Step 1 (Convection): All simulation particles move with their constant velocity for one time step Δt:

$$x_i^{n+1} = x_i^n + v_i^n \Delta t\,. \tag{25}$$

Step 2 (Weights): Weights b_0, b_1, b_2 can be obtained according to Eq. (21). And then, both N_c (the number of collision pairs to select) and N_M (the number of particles sampled from the Maxwellian) are calculated as

$$\begin{cases} N_c^n = \left\lfloor b_1 N^n \Big/ 2 + \chi_{N_c}^{n-1} \right\rfloor \\ N_M^n = \left\lfloor b_2 N^n + \chi_{N_M}^{n-1} \right\rfloor \end{cases}; \quad \chi_x^{n-1} = \begin{cases} 0, & t^n = 0 \\ x^{n-1} - \lfloor x^{n-1} \rfloor, & t^n = n\Delta t \end{cases} \tag{26}$$

where $\lfloor x \rfloor$ is the integer part of x.

Step 3 (Collision): Compute the collision term with the Monte Carlo method. It is noted that β is considered as a variable and updated at each time step if necessary in order to obtain a better estimation. In this computation, β is chosen as $\rho\sigma_{\max}$ which is the maximal cross area. The detail of the computation of the collision part used in the AP-DSMC is almost the same as that in DSMC.

Step 4 (Relaxation): Compute the Maxwellian term with Pullin's method [24]. The core idea of this method is to select the new velocity components from a normal distribution instead of the calculation of a large number of collisions in each cell. In order to achieve this goal, two important parameters have to be calculated first. The first one is the mass average velocity $\bar{u}$,

$$\bar{u}_j = \sum_{i=1}^{N_M} m_i v_{ij} \Big/ m_{tot} = \sum_{i=1}^{N_M} m_i v_{ij} \Big/ \sum_{i=1}^{N_M} m_i, \quad j = 1, 2, 3, \tag{27}$$

where m_{tot} is the total mass of the Maxwellian particles. The other one is e' which is defined as the total specific thermal energy stored in the single degree of freedom divided by the mass of one particle:

Table 2
Physical parameters for different species used in the numerical examples.

Number	gas	Symbol	m [10^{-27} kg]	d_{ref} [10^{-10} m]	T_{ref} [K]	ω
Species-1	Krypton	Kr	139.1	4.76	273	0.80
Species-2	Argon	Ar	66.3	4.17	273	0.81

$$\begin{cases} E' = \frac{1}{2}\sum_{j=1}^{3}\sum_{i=1}^{N_M} m_i v_{i,j} - \frac{1}{2}\sum_{j=1}^{N_M} m_i \sum_{j=1}^{3} \bar{u}_j, \\ \nu = \sum_{i=1}^{N_M} (3+\xi_i), \end{cases} \Rightarrow e'_{dof} = \frac{E'}{\nu}, \Rightarrow e' = \frac{N_s e'_{dof}}{m_s}, \tag{28}$$

where E' is the total thermal energy of all particles in the cell and ν is the total number of degrees of freedom. ξ is the number of fully excited degrees of freedom of the molecular structure ($\xi = 0$ for monatomic particles and $\xi = 2$ for diatomic species). Only monatomic particles are considered in this work. e'_{dof} is the mean thermal energy per single degree of freedom. N_s (satisfy $\sum_{s=1}^{N} N_s = N_M$) and m_s are the particle number and particle mass for one species respectively. After that, the new velocity components of the equilibrium particles are sampled in the way that the mean and variance of the finite sample conform to values determined by the requirement that the total energy and momentum be conserved [19].

4. Numerical examples

In this section, several examples with different purposes are chosen to test the developed multispecies AP-DSMC scheme. The aim of the first example is to test the effectiveness of the BGK-penalization for multispecies temperature relaxation. The next two one-dimensional examples (shock profile and Sod shock tube) are used to show the computational efficiency of our proposed scheme under different computational conditions. The proposed method's ability of effectively simulating the relatively complicated engineering problems with a large time step is demonstrated in the last example. As mentioned before, a large time step which satisfies $\Delta t > \varepsilon$ can be used in the proposed method due to its asymptotic preserving property. It should be noticed that both the $\Delta t = \Delta\tilde{t} \,/\, \tau = \Delta\tilde{t}\tilde{c} \,/\, L$ and the $\varepsilon = \lambda \,/\, L$ are dimensionless parameters in Eq. (3). The overall mean free path λ for a mixture of ns separate gas species is [1]

$$\begin{cases} \lambda = \sum_{p=1}^{ns} \frac{n_p}{n} \left\{ \sum_{q=1}^{ns} \left[\pi \left(d_{ref}\right)_{pq}^2 n_q \left(\frac{\left(T_{ref}\right)_{pq}}{T} \right)^{\omega_{pq}-\frac{1}{2}} \left(1+\frac{m_p}{m_q}\right)^{\frac{1}{2}} \right] \right\}^{-1} \\ \left(d_{ref}\right)_{pq} = \frac{\left(d_{ref}\right)_p + \left(d_{ref}\right)_q}{2};\ \left(T_{ref}\right)_{pq} = \frac{\left(T_{ref}\right)_p + \left(T_{ref}\right)_q}{2};\ \omega_{pq} = \frac{\omega_p + \omega_q}{2} \end{cases} \tag{29}$$

where number density n satisfies $\sum_{p=1}^{ns} n_p = n$. ω is the temperature exponent and it can also be used to determine the viscosity coefficient μ which is proportional to a power law temperature T^{ω}. The values of the reference diameter d_{ref}, reference temperature T_{ref}, temperature exponent ω and molecular mass m for each species are presented in Table 2. For simplicity but without loss of generality, the characteristic length L is set to be 1 and only two species with equal mass fraction (0.5) are considered in each example.

4.1. Temperature relaxation in a homogeneous gas

In the first example, we consider a two monatomic species model with different initial conditions evolving to an equilibrium state. Due to the homogeneous spatial distribution, this example can be considered as a "zero-dimensional problem" and thus only one cell in the physical space is needed. The initial velocities for each species are obtained by sampling from the Maxwellian distribution functions. First, initial data with only different temperature for each species are given as follows

$$\text{Case 1}: \begin{cases} T_1 = 600\ \text{K};\ n_1 = 1.144\times 10^{21}/1.144\times 10^{24};\ u_1 = 0\ \text{m/s}, \\ T_2 = 400\ \text{K};\ n_2 = 1.144\times 10^{21}/1.144\times 10^{24};\ u_2 = 0\ \text{m/s}. \end{cases} \tag{30}$$

In order to obtain accurate solutions, a large number of particles ($N_p = 50\,000$) in the cell are used for both AP-DSMC and DSMC. We choose time step ($\Delta\tilde{t} = 2.417\times 10^{-7}$ s) and the corresponding dimensionless time step ($\Delta t = 1.0\times 10^{-4}$) can be obtained easily according to Table 1. The Knudsen number ε are 1×10^{-3} and 1×10^{-6} respectively for these two different number densities. Temperature relaxation processes of these two species calculated by AP-DSMC and DSMC method are compared in Fig. 2. It can be found that the AP-DSMC results are in good agreement with DSMC results for these two cases with different ε: the temperature of each species ($T_1; T_2$) gradually converges to a mean temperature (about 500 K) and the smaller ε gives a faster convergence rate due to more collisions during one time step.

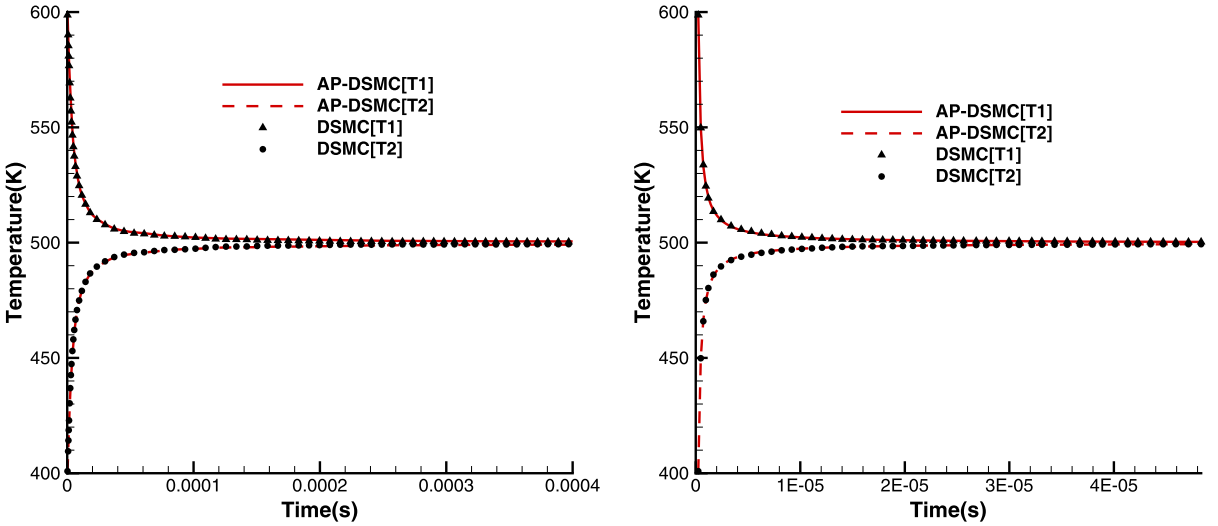

Fig. 2. Temperature relaxation in a homogenous gas for Case 1. Left: $\varepsilon = 1.0 \times 10^{-3}$; Right: $\varepsilon = 1.0 \times 10^{-6}$. T1 and T2 represent the temperature for species 1 and species 2 respectively.

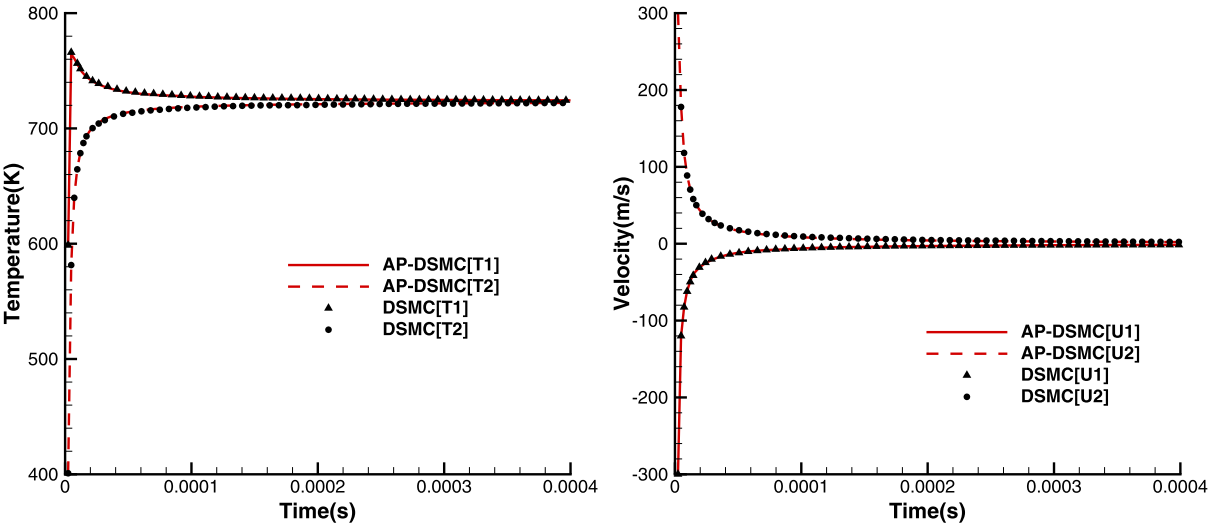

Fig. 3. Relaxation in a homogenous gas for Case 2. Left: Temperature; Right: Velocity. U1 and U2 represent the velocity for species 1 and species 2 respectively.

$$\text{Case 2}: \begin{cases} T_1 = 600\ \text{K};\ n_1 = 1.144 \times 10^{24};\ u_1 = -300\ \text{m/s}, \\ T_2 = 400\ \text{K};\ n_2 = 1.144 \times 10^{24};\ u_2 = 300\ \text{m/s}. \end{cases} \tag{31}$$

Next, another initial data with different velocity are used to test the AP-DSMC. In this case, time step and particle number are the same as those used in Case 1. The results are given in Fig. 3. It can be found that the numerical results obtained by the AP-DSMC again match well with those computed by the DSMC. Therefore, the numerical results show that the proposed AP-DSMC has the ability to handle the multispecies relaxation problems even if Δt is greatly larger than ε.

Although the numerical results obtained by these two methods are almost the same, the computational costs are quite different with different ε. Take the case-1 for example, the total execution time of AP-DSMC and DSMC for $\varepsilon = 1 \times 10^{-3}$ are 5.6 s and 6.7 s respectively. However, when ε is 1×10^{-6}, the computational time of AP-DSMC (32.8 s) is much less than that of DSMC (223.6 s). More thorough discussions about the comparison computational efficiency between AP-DSMC and DSMC will be presented in the next two examples.

4.2. Stationary shock structure

In the second example, an one-dimensional stationary shock profile of two species at different shock Mach numbers is simulated by the proposed AP-DSMC. The DSMC1S.FOR [1] is used to compute the reference solutions. The computational

Table 3
Comparison between dimensionless time step and Knudsen number for Example 2.

Case	Ma	$\Delta\tilde{t}$ [s]	T [K]	$\bar{c}$ [m/s]	Δt	ε	$\Delta t \,/\, \varepsilon$
1	2	2.0×10^{-5}	608.9	456.6	9.13×10^{-3}	6.25×10^{-3}	1.46
2	4	2.0×10^{-5}	1717.9	766.9	1.53×10^{-2}	5.82×10^{-3}	2.64
3	6	2.0×10^{-5}	3551.1	1102.6	2.21×10^{-2}	6.63×10^{-3}	3.33
4	8	2.0×10^{-5}	6115.5	1466.9	2.89×10^{-2}	7.56×10^{-3}	3.83

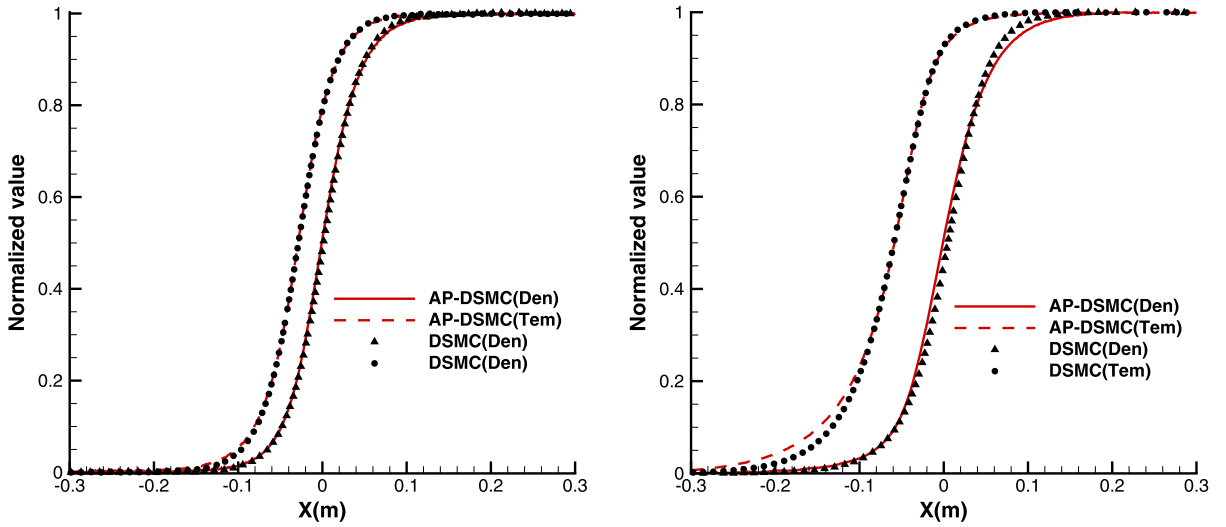

Fig. 4. The stationary shock profile with different Mach numbers for Example 2. Left: Mach = 2; Right: Mach = 8; Den and Tem represent density and temperature respectively. All the values are normalized by the initial data.

domain is $[-0.3\text{ m}, 0.3\text{ m}]$ with the mesh number $N = 600$. The boundary conditions are farfield conditions. The number density n and temperature T in the upstream side ($x < 0$) are 1.0×10^{20} and 293 K respectively. Four Mach numbers ($Ma = 2.0, 4.0, 6.0, 8.0$) are considered in this example. The time step is $\Delta\tilde{t} = 2 \times 10^{-5}$ s and 100 particles per cell are given in the upstream. According to the Mach number and the Rankine–Hugoniot relations, the initial data and the particle number in each cell in the downstream can be computed. See Table 3 for other computational parameters. The numerical results obtained by AP-DSMC are DSMC are averaged by 1×10^4 samples.

Fig. 4 shows the stationary shock structures obtained by the AP-DSMC and DSMC1S.FOR at different Mach numbers. The numerical results indicate very good agreement with each other in all cases. Like DSMC scheme, AP-DSMC has the ability to capture the correct size of the separation between density and temperature in a shock, which is caused by the finite relaxation times for momentum and energy transport. Furthermore, the computational efficiency of these two methods are studied. The detailed computational CPU time of AP-DSMC and DSMC are shown in Table 4 and in Fig. 6 (left). In the left of the Fig. 6, the computational CPU times of each case is normalized with the total time of DSMC in the case with Mach = 1. It can be found that the total time of AP-DSMC is composed of the convection time, collision time and relaxation time, while the total time of DSMC comprises of the convection time and collision time. We can see that the computational costs of these two methods increase as the Mach number increase and AP-DSMC saves more computing time than the DSMC in the case with larger Mach numbers. For Case 4, the computing time of AP-DSMC is around 50% less than that of DSMC. In Fig. 5 (left), one can find the reasons for high computational efficiency of AP-DSMC with large Mach numbers. One the one hand, increasing the velocity leads to more collisions during a time step; on the other hand, a higher mach number causes higher density in the downstream region ($x > 0$) according to the Rankine–Hugoniot relations. As a result, more time-consuming collision process (controlled by b2) will be transferred to the relaxation process (controlled by b3) in the cases with larger Mach numbers.

4.3. Shock tube: Sod problem

In this example, Sod's shock tube problem is applied to test the AP-DSMC's capability of capturing unsteady profiles and to show the advantage in computational efficiency with various Knudsen number, compared with DSMC. The computational domain is $[0, 0.01\text{ m}]$ with a unified mesh of $N = 500$ and the time step is $\Delta\tilde{t} = 1 \times 10^{-6}$ s. The initial data are given by

$$\begin{cases} p = \xi\text{ Pa},\ T = 300\text{ K},\ u = 0\text{ m/s} & x \le 0.005\text{ m}, \\ p = 0.125\xi\text{ Pa},\ T = 300\text{ K},\ u = 0\text{ m/s} & x > 0.005\text{ m}. \end{cases} \tag{32}$$

Table 4
Comparisons of computational CPU time (minutes) taken by different methods for Example 2. Percentage means the ratio of AP-DSMC' total time to the corresponding DSMC's total time.

Mach	Method	Convection	Collision	Relaxation	Total time	Percentage
2.0	AP-DSMC	1.98	5.07	5.45	20.11	72.78%
2.0	DSMC	1.96	18.39	–	27.62	–
4.0	AP-DSMC	2.64	6.03	10.77	29.29	60.51%
4.0	DSMC	2.60	36.88	–	48.40	–
6.0	AP-DSMC	2.97	5.87	12.89	31.74	53.89%
6.0	DSMC	2.91	46.95	–	58.89	–
8.0	AP-DSMC	3.11	5.32	15.23	32.49	46.31%
8.0	DSMC	3.09	60.04	–	70.17	–

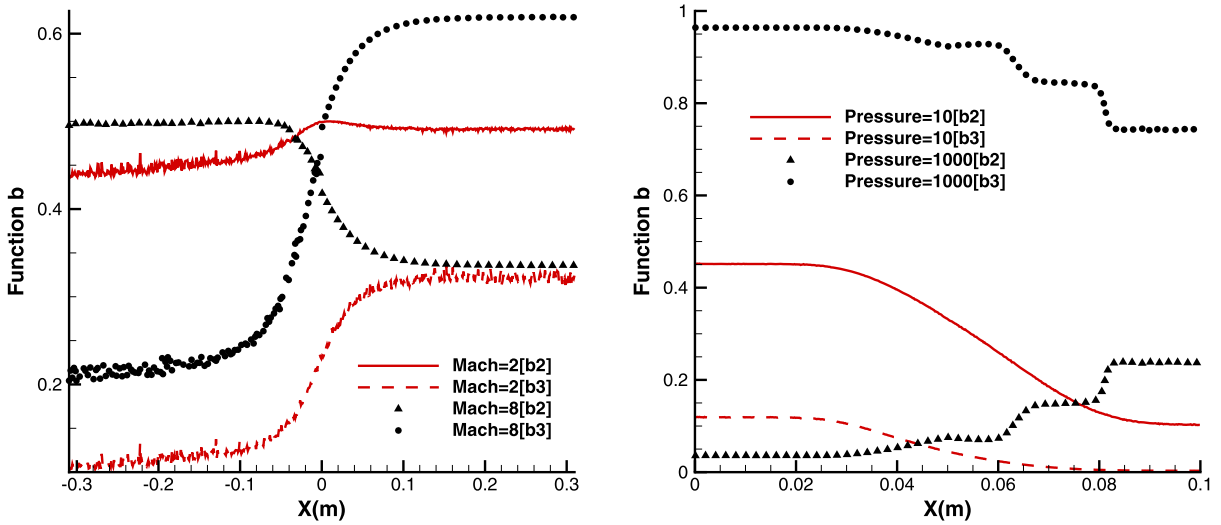

Fig. 5. Comparison of function b for different examples. Left: Example 2; Right: Example 3. It should be noted that the function b2 and b3, whose specific expressions are shown in Eq. (21), represent the weight coefficient for the collision process and the relaxation process respectively.

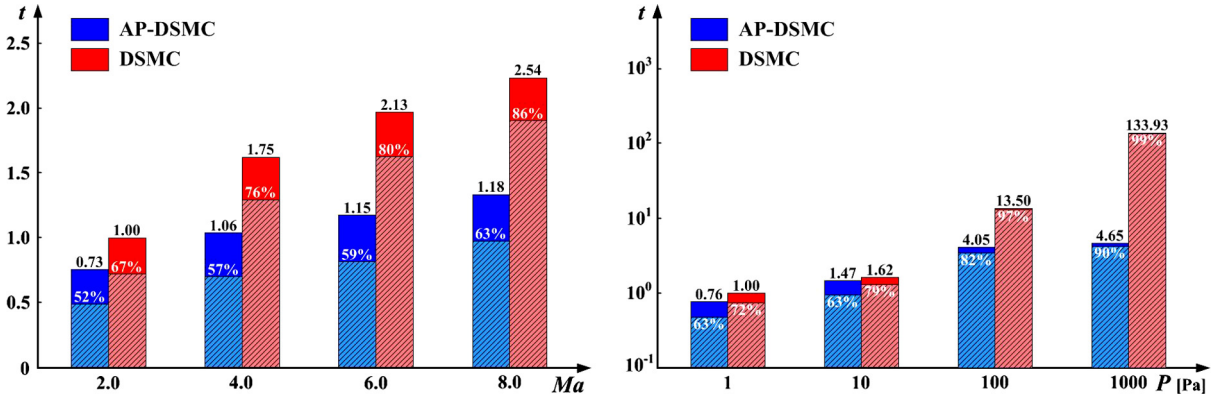

Fig. 6. Comparisons of normalized computational CPU time for different examples. Left: Example 2; Right: Example 3; The shadowed region in each red or blue bar represents the percentage of the collision time from the total time. Take the case with pressure = 1 example, the normalized total computational CPU time is 1, while the number 72% in the red bar means the normalized total computational CPU time of the collision process is about 0.72. (For interpretation of the references to color in this figure legend, the reader is referred to the web version of this article.)

Different Knudsen numbers listed in Table 5 can be obtained by choosing different $\xi = 1, 10, 100, 1000$. Both AP-DSMC and DSMC use the same particle number ($N_p = 50$ in each cell of upstream regime and the corresponding particle number in each cell of downstream regime can be calculated with the flowfield parameters) and sample number ($N_s = 1000$). The computation stops at $\tilde{t} = 8 \times 10^{-4}$ s. Fig. 7 shows the comparisons of the numerical results of AP-DSMC and DSMC with different ε (from rarefied to continuum) regimes. The numerical results (pressure and temperature) are normalized with reference values (ξ and 300 K). Fig. 7 indicates that both AP-DSMC and DSMC can capture the positions and profiles of the expansion wave, contact discontinuity and the shock wave from rarefied to continuum regimes. Next, we will focus on the

Table 5
Comparison between dimensionless time step and Knudsen number for Example 3.

Case	P [Pa]	$\Delta\tilde{t}$ [s]	T [K]	$\bar{c}$ [m/s]	Δt	ε	$\Delta t/\varepsilon$
1	1	1.0×10^{-6}	300.0	320.5	3.2×10^{-4}	4.77×10^{-3}	0.067
2	10	1.0×10^{-6}	300.0	320.5	3.2×10^{-4}	4.77×10^{-4}	0.67
3	100	1.0×10^{-6}	300.0	320.5	3.2×10^{-4}	4.77×10^{-5}	6.7
4	1000	1.0×10^{-6}	300.0	320.5	3.2×10^{-4}	4.77×10^{-6}	67.0

Table 6
Comparisons of computational CPU time taken by different methods for Example 3. Percentage means the ratio of AP-DSMC' total time to the corresponding DSMC's total time.

Knudsen number	Method	Convection	Collision	Relaxation	Total time	Percentage
4.8×10^{-1}	AP-DSMC	3.5	0.6	2.8	14.2	120.3%
4.8×10^{-1}	DSMC	3.3	2.4	–	11.8	–
4.8×10^{-2}	AP-DSMC	3.0	9.8	6.7	26.1	90.9%
4.8×10^{-2}	DSMC	3.2	22.8	–	28.7	–
4.8×10^{-3}	AP-DSMC	4.0	9.4	49.4	71.6	30.0%
4.8×10^{-3}	DSMC	3.9	231.7	–	238.9	–
4.8×10^{-4}	AP-DSMC	4.2	2.1	72.0	82.3	3.5%
4.8×10^{-4}	DSMC	4.0	2364.4	–	2370.6	–

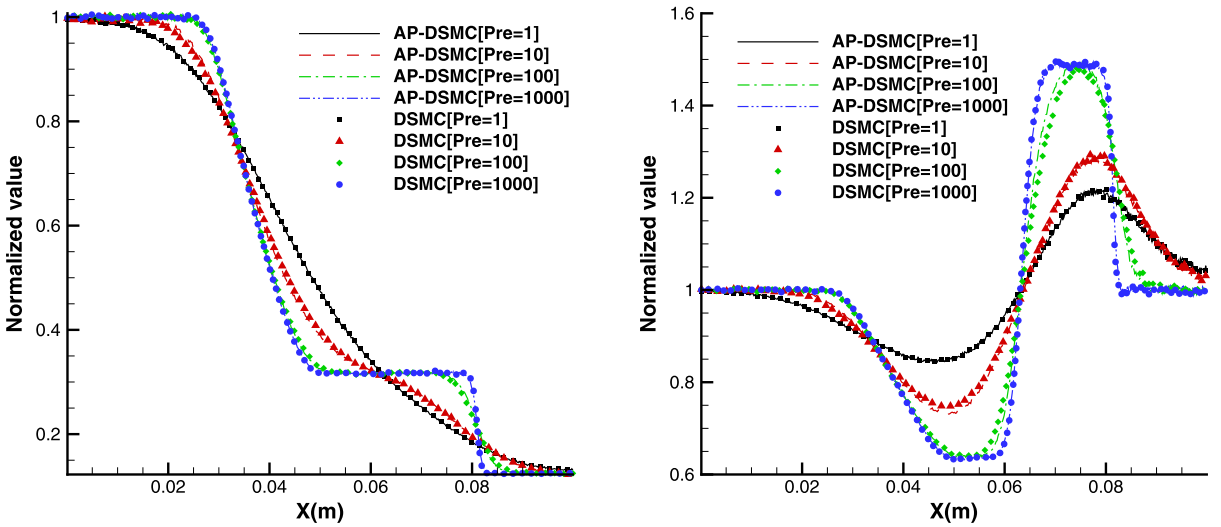

Fig. 7. Comparison of normalized results with different pressures for Example 3. Left: Pressure, Right: Temperature. Pre represents pressure.

comparison of computational efficiency. Table 6 and Fig. 6 (right) show the detailed computational CPU time of AP-DSMC and DSMC. In the right of the Fig. 6, the computational CPU times of each case is normalized with the total time of DSMC in the case with pressure = 1. When ε is very large, there is little difference between AP-DSMC and DSMC in computational efficiency. It should be noted that AP-DSMC costs about 20% CPU time more than DSMC in Case 1. The reason is that the relaxation part costs more computational time than the collision part if ε is large. As ε decreases, the computational cost of DSMC starts to soar because the small ε leads to large number of collisions. Thus most of computing time has to be spent on resolving the collision process. However, in this situations, an appropriate relaxation process replaces most parts of collision in AP-DSMC (see right subfigure of Fig. 5). Take Case 4 for example, the computing time taken by DSMC is almost twenty-night times as much as that of AP-DSMC. Therefore, it can be concluded that AP-DSMC is much more efficient than DSMC when ε is vanishing.

4.4. The interaction of jets with crossflow

The studies of high-speed jets in crossflow mostly consider application to thrust vectoring for hypersonic vehicles [20]. Generally, a very large range of ε exists in this multispecies flowfield, which provides an appropriate case to test the proposed method. Just as shown in Fig. 8 (left), the two dimensional computational domain is split into three sub-regions. The A, B and C sub-regions are divided into 600×400, 60×400 and 800×400 cells respectively. The diffusive boundary condition (the velocities of the reflected molecules are distributed in accordance with the Maxwellian distribution) is applied on the wall and the wall temperature is fixed at 300 K. The computations are initialized with at least 5 particles in the

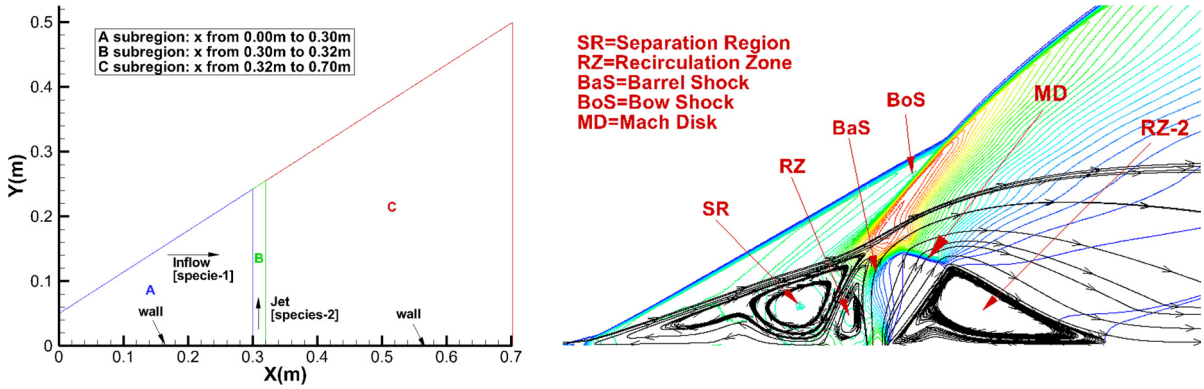

Fig. 8. Schematic plot for the interaction of jet with crossflow problem. Left: computational domain, Right: streamline of the flow obtained by AP-DSMC with time step $\Delta\tilde{t} = 5 \times 10^{-8}$ s.

Table 7
The computational parameters in Example 4.

–	Pressure [Pa]	Temperature [K]	Mach number	Angle [°]	Species
Inflow	200.0	300.0	8.0	0.0	Kr
Jet	5000.0	600.0	2.0	90.0	Ar

Table 8
Comparisons of computational CPU time (hour) taken by different time steps for Example 4.

Case	$\Delta\tilde{t}$	$\Delta t \,/\, \varepsilon$	Convection	Collision	Sample	Total time
1	1.0×10^{-7} s	23.7	5.6	12.5	2.8	27.8
2	5.0×10^{-8} s	11.8	6.8	14.4	4.2	36.6
3	1.0×10^{-8} s	2.4	25.5	26.1	19.3	118.5

minimal cell. The computational parameters related to the inflow and jet flow are listed in Table 7. Only AP-DSMC is used for this example since DSMC is almost impossible due to the tremendous computation costs caused by the small time step. In this example, three relatively large time steps $\Delta\tilde{t} = 1 \times 10^{-8}, 5 \times 10^{-8}, 1 \times 10^{-7}$ s are compared and their corresponding dimensionless time step are larger than the Knudsen number ($\varepsilon = 1.65 \times 10^{-6}$) which is calculated with the jet flow parameters. The flowfields for these three different time steps reach steady-state after about 450 000, 90 000, 45 000 samples respectively. The output results are averaged by the subsequent 50 000 samples.

Fig. 8 (right) shows some basic flow characteristics of the interaction between jets and the crossflow. A bow shock forms ahead of the jet due to the low momentum of the jet fluid relative to the crossflow, barrel shocks are observed at its periphery, and the jet fluid forms a Mach disk as it expands into and bends toward the crossflow. The interaction of the bow shock wave with the portion of the upstream boundary layer causes the flow to separate. In the recirculation zones, the high momentum gas is convected from the freestream down to the wall. Fig. 9 and Fig. 10 show the contour of macroscopic quantities and jet particles distribution for AP-DSMC with $\Delta\tilde{t} = 5 \times 10^{-8}$ respectively. It can be found that more relaxation processes are needed in the areas near the jet exit and shocks. Both the pressure and heat transfer coefficients [1] on the wall defined as follows are used to give a further comparison,

$$C_p = \frac{2p}{\rho_\infty u_\infty^2}, \; C_H = \frac{2\rho q_w}{\rho_\infty u_\infty^3}, \tag{33}$$

where subscript p and H denote pressure and heat transfer respectively. ρ_∞ and u_∞ are the density and velocity magnitudes of the inflow. Fig. 11 shows the comparison of wall information obtained by AP-DSMC with different time steps. Except few differences near the peak of heat transfer, the wall information obtained with different time steps are similar. As explained in [25], it is hard for the schemes based on projection onto a Maxwellian to capture the peak heat flux value with a small deviation from a Maxwellian. Finally, in order to show the advantage of AP-DSMC with large time step in computational efficiency, the comparisons of computational CPU time with different time steps are shown in Table 8 in details. Due to the huge computational costs, the computations of these cases are conducted under the MPI parallel environment (using 64 cores). We can see that Case 1, Case 2 and Case 3 cost 27.8, 36.6 and 118.5 hours respectively. The case with small time step has to use more samples to confirm that the flowfield has already reached the stead state. If time step satisfies the relation of $\Delta t \ll \varepsilon$ as in DSMC, more samples are required and this will lead to the soar of computational cost. Therefore, this example demonstrates that AP-DSMC with large time step is very promising in real-world engineering applications.

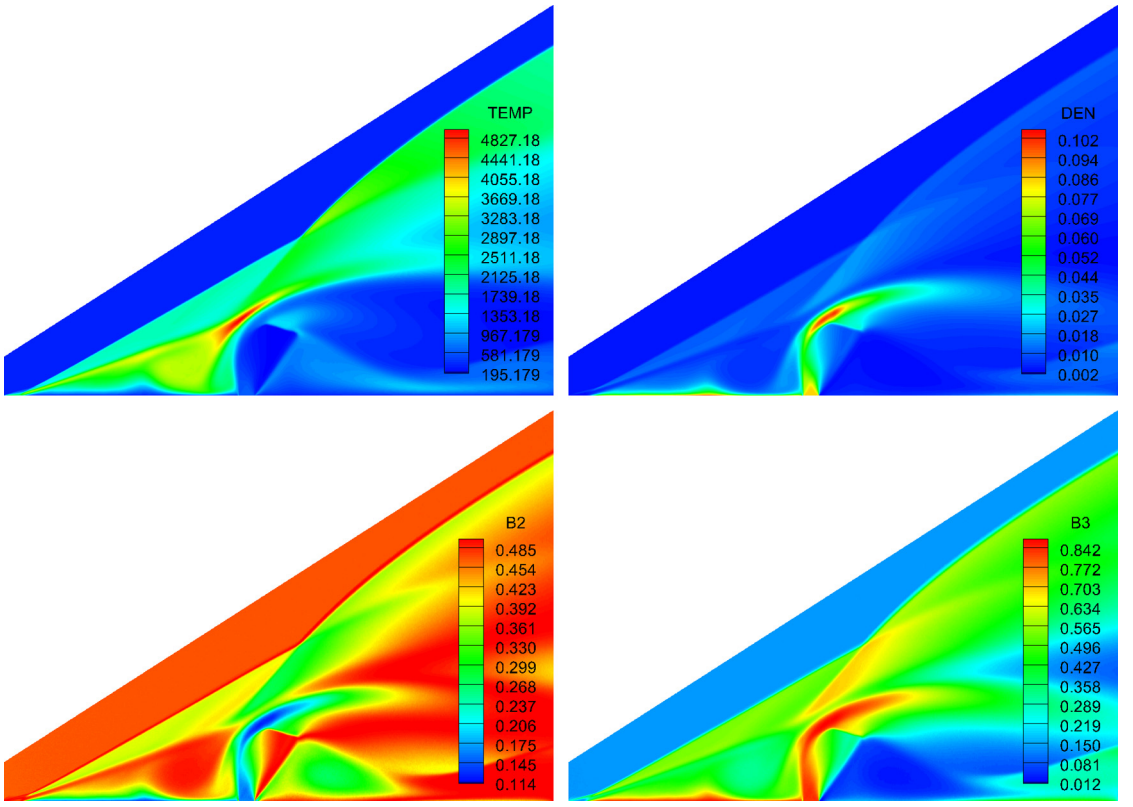

Fig. 9. Contour of macroscopic quantities for AP-DSMC with time step $\Delta\tilde{t} = 5 \times 10^{-8}$ s. Top left: Temperature, Top right: Density, Bottom left: Function b_2, Bottom right: Function b_3.

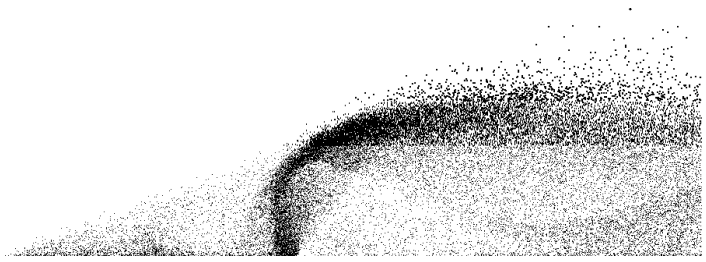

Fig. 10. Distribution of jet particles for AP-DSMC with time step $\Delta\tilde{t} = 5 \times 10^{-8}$ s.

5. Conclusion

In this paper, we extend the asymptotic preserving Monte Carlo method, originally introduced in [25] for the single species Boltzmann equation, to its multispecies counterpart. In order to overcome the new difficulty coming from the breaking down of the conservation laws for each species due to the interaction between different species, as was done in [12], we use an appropriate BGK operator which is defined by the mean velocity and mean temperature to penalize the stiff collision operator for multispecies Boltzmann equation. Several numerical examples are used to test the proposed method by comparing it with the conventional DSMC method. Numerical results show that the proposed method not only has the ability to capture the hydrodynamic limit, but also allows the time step to be independent of the Knudsen number. Thus, this AP scheme is very suitable for simulating the multispecies Boltzmann equation efficiently in both the kinetic and fluid regimes. In the future, we will work on developing the AP Monte Carlo scheme for diatomic molecular simulations and applying the proposed method in more complicated engineering problems.

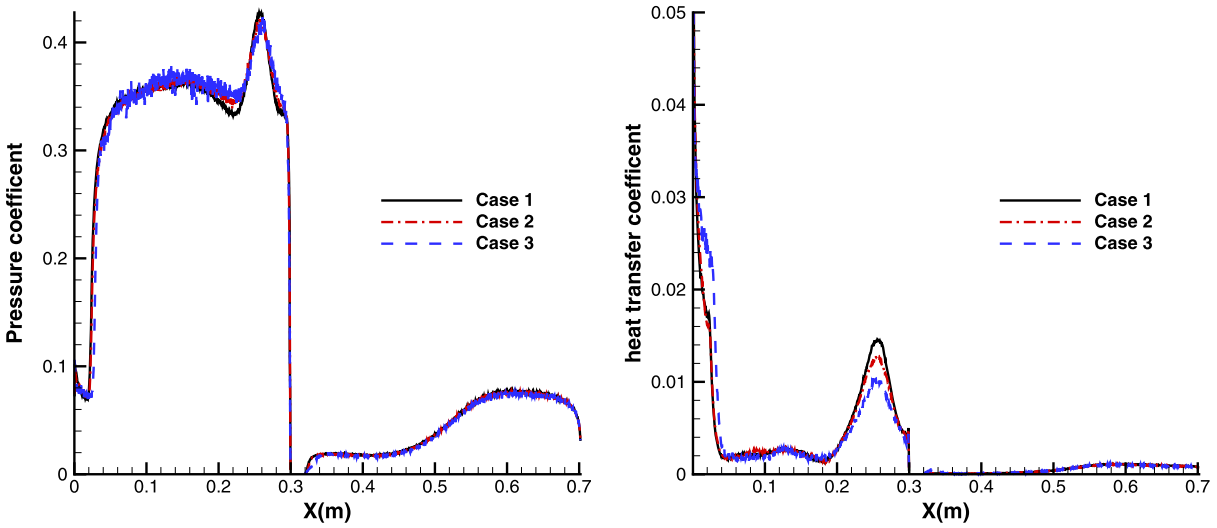

Fig. 11. Comparison of wall information of AP-DSMC with different time steps. Left: pressure coefficient, Right: heat transfer coefficient.

Acknowledgements

Thanks to the Center for High Performance Computing of SJTU for providing the super computer "π" to support this research. This work was partially supported by the National Natural Science Foundation of China (NSFC-91330203 and NSFC-91441205) and the China Postdoctoral Science Foundation (2015M571560).

References

[1] G.A. Bird, Molecular Gas Dynamics and the Direct Simulation Monte Carlo of Gas Flows, Clarendon, Oxford, 1994, 508.
[2] J.F. Bourgat, P. Le Tallec, B. Perthame, Y. Qiu, Coupling Boltzmann and Euler equations without overlapping, Contemp. Math. 157 (1994) 377–398.
[3] P. Degond, S. Jin, A smooth transition model between kinetic and diffusion equations, SIAM J. Numer. Anal. 42 (2005) 2671–2687.
[4] P. Degond, S. Jin, L. Mieussens, A smooth transition model between kinetic and hydrodynamic equations, J. Comput. Phys. 209 (2005) 665–694.
[5] G. Dimarco, L. Pareschi, Exponential Runge–Kutta methods for stiff kinetic equations, J. Comput. Phys. 49 (2011) 2057–2077.
[6] G. Dimarco, L. Pareschi, Numerical methods for kinetic equations, Acta Numer. 23 (2014) 369–520.
[7] F. Filbet, S. Jin, A class of asymptotic-preserving schemes for kinetic equations and related problems with stiff sources, J. Comput. Phys. 229 (2010) 7625–7648.
[8] E. Gabetta, L. Pareschi, G. Toscani, Relaxation schemes for nonlinear kinetic equations, SIAM J. Numer. Anal. 34 (1997) 2168–2194.
[9] F. Golse, S. Jin, C.D. Levermore, A domain decomposition analysis for a two-scale linear transport problem, Math. Model. Numer. Anal. 37 (37) (2002) 869–892.
[10] S. Jin, Efficient asymptotic-preserving (ap) schemes for some multiscale kinetic equations, SIAM J. Sci. Comput. 21 (1999) 441–454.
[11] S. Jin, Asymptotic preserving (ap) schemes for multiscale kinetic and hyperbolic equations: a review, in: Lecture Notes for Summer School on Methods and Models of Kinetic Theory (M&MKT), Porto Ercole (Grosseto, Italy), in: Riv. Mat. Univ. Parma, 2010, pp. 177–216.
[12] S. Jin, Q. Li, A bgk penalization-based asymptotic-preserving scheme for the multispecies Boltzmann equation, Numer. Methods Partial Differ. Equ. 29 (2013) 1056–1080.
[13] S. Jin, X. Yang, G. Yuan, A domain decomposition method for a two-scale transport equation with energy flux conserved at the interface, Kinet. Relat. Models 1 (2008) 65–84.
[14] K.C. Kannenberg, I.D. Boyd, Strategies for efficient particle resolution in the direct simulation Monte Carlo method, J. Comput. Phys. 157 (2000) 727–745.
[15] A. Klar, H. Neunzert, J. Struckmeier, Transition from kinetic theory to macroscopic fluid equations: a problem for domain decomposition and a source for new algorithms, J. Comput. Phys. 29 (2000) 93–106.
[16] E.W. Larsen, J.E. Morel, Asymptotic solutions of numerical transport problems in optically thick, diffusive regimes ii, J. Comput. Phys. 83 (1989) 212–236.
[17] C. Liu, K. Xu, Q. Sun, Q. Cai, A unified gas-kinetic scheme for continuum and rarefied flows, direct modeling, and full Boltzmann collision term, arXiv:1405.4479, 2014.
[18] M.N. Macrossan, The equilibrium flux method for the calculation of flows with non-equilibrium chemical reactions, J. Comput. Phys. 80 (1989) 204–231.
[19] M.N. Macrossan, Some developments of the equilibrium particle simulation method for the direct simulation of compressible flows, DTIC Document, 1995.
[20] K. Mahesh, The interaction of jets with crossflow, Annu. Rev. Fluid Mech. 45 (2013) 379–407.
[21] L. Pareschi, R.E. Caflisch, An implicit Monte Carlo method for rarefied gas dynamics: I. The space homogeneous case, J. Comput. Phys. 154 (1999) 90–116.
[22] L. Pareschi, G. Russo, Time relaxed Monte Carlo methods for the Boltzmann equation, SIAM J. Sci. Comput. 23 (2001) 1253–1273.
[23] L. Pareschi, S. Trazzi, Numerical solution of the Boltzmann equation by time relaxed Monte Carlo(trmc) methods, Int. J. Numer. Methods Fluids 48 (2005) 947–983.
[24] D.I. Pullin, Direct simulation methods for compressible inviscid ideal-gas flow, J. Comput. Phys. 34 (1980) 231–244.
[25] W. Ren, H. Liu, S. Jin, An asymptotic-preserving Monte Carlo method for the Boltzmann equation, J. Comput. Phys. 276 (2014) 380–404.
[26] B. Yan, S. Jin, A successive penalty-based asymptotic-preserving scheme for kinetic equations, SIAM J. Sci. Comput. 35 (2013) 150–172.